COMMUN. MATH. SCI.
Vol. 12, No. 7, pp. 1329–1342

FAST COMMUNICATION

TOPOLOGY PRESERVING ACTIVE CONTOURS*

HAYDEN SCHAEFFER†, NÓIRÍN DUGGAN‡, CAROLE LE GUYADER§, AND LUMINITA VESE¶

Abstract. Active contours models are variational methods for segmenting complex scenes using edge or regional information. Many of these models employ the level set method to numerically minimize a given energy, which provides a simple representation for the resulting curve evolution problem. During the evolution, the curve can merge or break, thus these methods tend to have steady state solutions which are not homeomorphic to the initial condition. In many applications, the topology of the edge set is known, and thus can be enforced. In this work, we combine a topology preserving variational term with the region based active contour models in order to segment images with known structure. The advantage of this method over current topology preserving methods is its ability to locate boundaries of objects and not only edges. This is particularly useful for highly textured or noisy data.

Key words. Active contour, topology preserving, region based models, non-local PDE.

AMS subject classifications. 68U10, 65K10.

1. Introduction

Active contour methods segment images by evolving a curve until it captures either boundaries and/or edges. The curve dynamics are typically defined to descend a specified energy towards the minimizer. In general, the energy contains information on the desired structure of the curve as well as quantitative measures of edges and boundaries. In many applications, the topological structure of the edge set is known *a priori* and thus can be embedded in the initial curve. Therefore, we would want the final solution to be homeomorphic to the initial data, although in the popular level set based methods this cannot be guaranteed. Some works in the literature (for example, [7, 10]) have incorporated forcing terms to prevent the change in topology that occurs during the curve evolution process, but mainly focus on locating edges. In this way, those methods are (in some sense) interpolating edge detector information under the condition that some known structure must be preserved. In this work, we show that by using regional information one is able to segment the image while constraining the topology. Our main contribution is the combination of region based active contour models with topological forces.

The first active contour model (Snakes) [8] used a variational method to find the edges in an image f. Defining the domain as $\Omega \subset \mathbb{R}^2$ and the edge set as a curve

*Received: August 15, 2013; accepted (in revised form): December 10, 2013. Communicated by Richard Tsai.

†520 Portola Plaza, Math Sciences Building 6363, Los Angeles, CA 90095, USA (hschaeffer@ucla.edu).

‡Electrical and Electronic Engineering Building, National University of Ireland, Galway, Ireland (nduggan@math.ucla.edu).

§INSA Rouen, Laboratory of Mathematics, 685 Avenue de l'Université, 76801 Saint-Etienne-du-Rouvray Cedex, France (carole.le-guyader@insa-rouen.fr).

¶520 Portola Plaza, Math Sciences Building 6363, Los Angeles, CA 90095, USA (lvese@math.ucla.edu).

$\mathcal{C}:[0,1]\to\mathbb{R}^2$, then the Snakes model is defined below:

$$E_S(\mathcal{C}(s))=\int_0^1\left(\gamma_1|\mathcal{C}'|^2+\gamma_2|\mathcal{C}''|^2\right)ds-\int_0^1|\nabla f(\mathcal{C})|^2ds, \tag{1.1}$$

where $\gamma_1,\gamma_2>0$ are smoothing parameters. The first two terms determine the smoothness of the curve $\mathcal{C}$, while the last term keeps the curve close to the edges. Essentially, the last term in equation (1.1) is a variational edge detector that encourages the curve to remain along pixels with sharp gradients. A general edge detector is defined as a function $g(|\nabla f|)$ which decays to 0 as $|\nabla f|$ goes to infinity. Typically, g is small for large arguments and nearly 1 for small arguments, thereby acting as a smoothed edge indicator function.

The geodesic active contours (GAC) model [2, 9] determines the edge set by finding the geodesics of the function g defined above. Using the function g, the geodesic energy is defined as

$$E_{GAC}(\mathcal{C})=\int_0^1 g(|\nabla f(\mathcal{C}(s))|)|\mathcal{C}'(s)|ds \tag{1.2}$$

and represents the length functional with respect to the new edge metric. The curve is drawn to pixels in which $g(|\nabla f(\mathcal{C}(s))|)$ is close to zero.

While both the Snakes and GAC models measure the edge set via sharp gradients, the Mumford and Shah (MS) model [11] segments the image based on regional information as well as reconstructs a piecewise smooth approximation to the given data. By minimizing

$$E_{MS}(u,\mathcal{C})=\mu\int_{\Omega\setminus\mathcal{C}}|\nabla u|^2dx+\gamma\int_\Omega|u-f|^2dx+\mathcal{H}^1(\mathcal{C}), \tag{1.3}$$

the MS model approximates f by u as well as finds the edge set $\mathcal{C}$ which leaves u smooth. From the MS model perspective, the edge set is the set of boundaries between the smooth regions in the image.

In many cases, the image is well-approximated by a piecewise constant function. With this in mind, the Chan-Vese (CV) model [4] approximates f by a binary function, which is equal to c_1 in the interior of the region defined by curve $\mathcal{C}$ and c_2 in the exterior of the region defined by curve $\mathcal{C}$. The associated energy is

$$E_{CV}(c_1,c_2,\mathcal{C})=\gamma\int_{int(\mathcal{C})}|f-c_1|^2dx+\gamma\int_{int(\mathcal{C})^c}|f-c_2|^2dx+\nu\text{Length}(\mathcal{C}), \tag{1.4}$$

and minimizers of this energy are binary functions whose discontinuity set is small. The MS and CV models have many extensions, for example to vector valued images in [3], to 4 or more regions [17], to multilayer images in [5], and to curves with free endpoints [15, 16].

In practice, it is possible to get solutions of equation (1.4) to be homeomorphic to the initial condition; for example see the Gestalt theoretical solutions in [4]. However, these solutions are typically local minimizers of the functional above (due to the non-convex structure of the energy). In order to guarantee preservation of the curve topology during its evolution, an additional variational term must be included.

In [7], the authors proposed to use a topology-preserving level set method in order to prevent the topological changes common to the framework. Their method relies on the discrete representation of the curve on the pixel level. They proposed

examining the sign changes of the level set function over each of the pixels near the zero level curve to control the structural changes. By using the notation of simple points (those that can be removed without affecting the topology of the set), they build an algorithm which enforces fixed topology. Thus as the curve evolves, the algorithm monitors sign changes and prevents structural changes.

For level set based shape optimization, [1] proposed using the following logarithmic barrier functional to enforce constant topology:

$$\mathcal{H}(\phi) = -\int_{\mathcal{C}} \log[\phi(x + d\nabla\phi(x))]\,\mathrm{ds} - \int_{\mathcal{C}} \log[-\phi(x - l\nabla\phi(x))]\,\mathrm{ds}, \tag{1.5}$$

where d and l are small positive constants and ϕ is a signed distance function whose zero level set is the curve $\mathcal{C}$. Equation (1.5) prevents sign changes from occurring near a band around the zero level curve defined by the normal directions and by the parameters d and l.

In [10], an alternative variational formulation is given for preserving the topology of level set based methods. The following energy was proposed:

$$T(\phi) := -\iint_{\Omega\times\Omega} \nabla\phi(x)\cdot\nabla\phi(y)\; G(\|x-y\|) W_l(\phi(x)) W_l(\phi(y))\;\mathrm{dx}\;\mathrm{dy}, \tag{1.6}$$

where $W_l(\phi(x)) = \chi_{\{x\in\Omega \;|\; |\phi(x)|\le l\}}$. In this formulation, the topological term is extended over a region via the W_l functions, rather than a contour integral as in previous methods. Topological changes are measured via gradients and the assumption is that opposite parallel gradients lead to structural changes (see Section 2.1 for more detail).

For edge detection, in [10] the GAC model was augmented by equation (1.6) to preserve structure during edge detection. The model is able to segment the image while remaining homeomorphic to the initial data, but relies on the edge detector in order to locate the proper edges. If the image contains noise, corruption, or texture, edge detection can become unreliable. In particular, because edge detectors rely on gradients to locate jumps, both noise and texture can make this task difficult. Also, when boundaries are not represented by sharp jumps, edge detectors are ineffective. To handle these more general cases, we use region based methods for robustness with the addition of equation (1.6) to enforce structure.

2. Description of proposed model

Our model is expressed within the level set framework proposed in [12]. A curve $\mathcal{C}$ is represented as the zero level set of a Lipschitz continuous function $\phi:\Omega\to\mathbb{R}$, *i.e.* $\mathcal{C} = \{x\in\Omega,\ \phi(x) = 0\}$. This implicit curve representation greatly simplifies the theoretical and practical implementation of the curve evolution process (as it descends towards the minimizer). For example, the length functional [6] can be written as

$$\mathrm{Length}(\mathcal{C}) = \int_{\Omega} |\nabla H(\phi)| \; = \int_{\Omega} \delta(\phi)|\nabla\phi|, \tag{2.1}$$

where H is the Heaviside function defined to be 1 for positive arguments and 0 otherwise and $\delta = H'$ is the Dirac delta measure. In order to differentiate equation (2.1) with respect to ϕ we must take a continuous approximation of δ. For example, parameterizing the approximation by $\epsilon > 0$, a standard approximation is $\delta_\epsilon(x) = \frac{1}{\pi}\frac{\epsilon}{\epsilon^2+x^2}$. Because ϵ must be taken at the grid resolution, for imaging problems it is commonly set to $\epsilon = 1$. For the rest of this work, we will assume that the following properties hold for the approximated Dirac delta function (dropping the subscript): 1. $\delta\in C^\infty$, 2. $\int \delta(x)dx = 1$, and 3. $\delta(x)\ge\beta>0$ for all x.

2.1. Topology preserving term. Let us recall the topological term from Section 1 which we use in our model. The variational term was proposed in [10] and is defined as

$$T(\phi) := -\iint_{\Omega\times\Omega} \nabla\phi(x)\cdot\nabla\phi(y)\; e^{-\frac{\|x-y\|^2}{d^2}} W_l(\phi(x))W_l(\phi(y))\;\mathrm{dx}\;\mathrm{dy}, \tag{2.2}$$

where $W_l(\phi(x)) := H(\phi(x)+l)H(l-\phi(x)) = \{x\in\Omega \mid |\phi(x)|\le l\}$ and ϕ is a signed distance function. Because the gradient of the function ϕ is normal to its level sets, the first term provides a measure of how close level sets are to intersecting each other. If the gradients are nearly anti-parallel, this indicates that the points x and y are from different neighborhoods of the curve and are likely to undergo a topological change. The anti-parallel condition is also the reason for the negative sign in equation (2.2). On the other hand, if the gradients are perpendicular to each other and the points are close to each other in space, then the points x and y are from the same segment of the curve. The exponential provides a reasonable definition of closeness of the points x and y. And lastly, the functions W_l extend the computational domain from the zero level set of ϕ to a neighborhood around the zero level set. In practice, this provides a buffer region around the curve and defines a minimal distance between different segments of the curve.

2.2. Our model. The proposed topology preserving active contours model is

$$\begin{aligned}&\min_{\phi,c_1,c_2} E(\phi,c_1,c_2)\\ &= \int_\Omega \delta(\phi)|\nabla\phi| \;+\mu\; T(\phi) \;+\gamma\; \int_\Omega \left[(f-c_1)^2H(\phi)+(f-c_2)^2H(-\phi)\right]\;\mathrm{dx}.\end{aligned} \tag{2.3}$$

In order to minimize equation (2.3), we take the first variation with respect to each variable. The second two variables c_j for $j=1,2$ are the regional means and are calculated as follows:

$$c_1 = \frac{\int_\Omega fH(\phi)\;\mathrm{dx}}{\int_\Omega H(\phi)\;\mathrm{dx}}, \tag{2.4}$$

$$c_2 = \frac{\int_\Omega fH(-\phi)\;\mathrm{dx}}{\int_\Omega H(-\phi)\;\mathrm{dx}}. \tag{2.5}$$

These expressions are the exact relationship given by the first variations. For the level set function, the standard technique is to embed the first variation of equation (2.3), with respect to ϕ, in an evolution equation. This yields the following:

$$\begin{aligned}\partial_t\phi = {}&\delta(\phi)\mathrm{div}\left(\frac{\nabla\phi}{|\nabla\phi|}\right) + 4\frac{\mu}{d^2}W_l(\phi)\int_\Omega (x-y)\cdot\nabla\phi(y)e^{-\frac{\|x-y\|^2}{d^2}}W_l(\phi(y))\;\mathrm{dy}\\ &+\gamma\delta(\phi)\left((f-c_2)^2-(f-c_1)^2\right),\end{aligned} \tag{2.6}$$

with Neumann boundary conditions. In equation (2.6), the first and third terms are concentrated along the curve, while the second term is acting nonlocally throughout the domain. To extend the support of the terms to the entire domain, we further rescale the PDE to

$$\partial_t\phi = |\nabla\phi|\mathrm{div}\left(\frac{\nabla\phi}{|\nabla\phi|}\right) + 4\frac{\mu}{d^2}W_l(\phi)\int_\Omega (x-y)\cdot\nabla\phi(y)e^{-\frac{\|x-y\|^2}{d^2}}W_l(\phi(y))\;\mathrm{dy}$$

$$+\gamma\left((f-c_2)^2-(f-c_1)^2\right). \tag{2.7}$$

The first term is the mean curvature of the zero level line (a common rescaling in the level set method), the second term is the topological force, and the last two terms are the regional forces. Notice that at steady state and under the assumption that $|\nabla\phi|=1$, equation (2.7) corresponds to the first variation of equation (2.3) along the zero level curve (*i.e.* the steady state of equation (2.6)). The motivation for this rescaling is to correctly balance the nonlocality of the topological force with the other terms in the evolution equation. The topological force plays two roles: it encourages a particular structure on the curve (*i.e.* the topology) as well as influences movement to different regions (*i.e.* a nonlinear force). Therefore, the topological term interacts with both the mean curvature (structure term) and the regional forces. From [10], the rescaling of the curvature term is well-behaved with the topology term. However, we must spread the influence of the regional forces in order to balance with the topological force. This is done by simply removing δ. Theorem 2.2 provides further justification for the rescaled equation.

REMARK 2.1. If μ is large relative to the other parameters (as well as larger than 1), then it is clear that the resulting evolution will not produce satisfactory results. However, the growth that occurs resembles the fingering effect seen in Hele-Shaw equations. This may be due to the self-repelling and competing dynamics of the topological force.

The rescaled model will descend a new energy, although the minimizer should be identical. The following theorem explains the rescaled equations descend behavior.

THEOREM 2.2. *Let $\phi(t,x)\in C^1([0,T];W^{1,\infty}(\Omega))$ be the solution to equation (2.7) with Neumann boundary conditions and $|\nabla\phi|=1$ a.e. in Ω. Then for all $t>0$, the evolution equation decreases an energy, i.e. $\partial_t\bar{E}(\phi)\le 0$, where the energy is defined below:*

$$\bar{E}(\phi)=\int_\Omega |\nabla\phi| \ +\mu\ T(\phi)\ +\gamma\ \int_\Omega ((f-c_1)^2-(f-c_2)^2)\phi\ \mathrm{dx}, \tag{2.8}$$

for fixed c_1 and c_2.

Proof. We can formally differentiate under the integral to find the energy's time derivative as follows (for simplicity, we drop the subscript on the integrals):

$$\begin{aligned}
&\partial_t\bar{E}(\phi(t,-))\\
&=\int \frac{\nabla\phi}{|\nabla\phi|}\cdot\nabla\phi_t\ \ \mathrm{dx}-\mu\iint\Big\{\left[\nabla\phi_t(x)\cdot\nabla\phi(y)+\nabla\phi(x)\cdot\nabla\phi_t(y)\right]\ e^{-\frac{\|x-y\|^2}{d^2}}W_l(\phi(x))W_l(\phi(y))\\
&\quad+\nabla\phi(x)\cdot\nabla\phi(y)\ e^{-\frac{\|x-y\|^2}{d^2}}\left[W_l'(\phi(x))W_l(\phi(y))\phi_t(x)+W_l(\phi(x))W_l'(\phi(y))\phi_t(y)\right]\Big\}\ \mathrm{dx\ dy}\\
&\quad+\gamma\ \int((f-c_1)^2-(f-c_2)^2)\phi_t\ \mathrm{dx}\\
&=\mathrm{Term}_1+\mathrm{Term}_2+\mathrm{Term}_3.
\end{aligned}$$

We will investigate this expression term by term. For the first term, integration by parts yields

$$\mathrm{Term}_1=\int\frac{\nabla\phi}{|\nabla\phi|}\cdot\nabla\phi_t\ \ \mathrm{dx}=-\int\mathrm{div}\left(\frac{\nabla\phi}{|\nabla\phi|}\right)\phi_t\ \mathrm{dx},$$

where boundary terms vanish because of the boundary conditions.

Lastly, the second term is made up of two subterms which we will handle separately:

$$\begin{aligned}\text{Term}_2 = &-\mu \iint \left[\nabla\phi_t(x)\cdot\nabla\phi(y)+\nabla\phi(x)\cdot\nabla\phi_t(y)\right]\ e^{-\frac{\|x-y\|^2}{d^2}} W_l(\phi(x))W_l(\phi(y)) \\ &+\nabla\phi(x)\cdot\nabla\phi(y)\ e^{-\frac{\|x-y\|^2}{d^2}}\Big[W_l'(\phi(x))W_l(\phi(y))\phi_t(x) \\ &+W_l(\phi(x))W_l'(\phi(y))\phi_t(y)\Big]\ \text{dx dy} \\ =&-\mu(\text{Term}_{2\text{a}}+\text{Term}_{2\text{b}}).\end{aligned}$$

The main task is to separate the variables x and y as done in [10]. This can be done via Fubini's theorem, by switching the order of integration and recombining terms to get

$$\begin{aligned}\text{Term}_{2\text{a}} &= \iint \left[\nabla\phi_t(x)\cdot\nabla\phi(y)+\nabla\phi(x)\cdot\nabla\phi_t(y)\right]\ e^{-\frac{\|x-y\|^2}{d^2}} W_l(\phi(x))W_l(\phi(y))\ \text{dx dy} \\ &= \iint \nabla\phi_t(x)\cdot\nabla\phi(y) e^{-\frac{\|x-y\|^2}{d^2}} W_l(\phi(x))W_l(\phi(y))\ \text{dx dy} \\ &\quad + \iint \nabla\phi(x)\cdot\nabla\phi_t(y)\ e^{-\frac{\|x-y\|^2}{d^2}} W_l(\phi(x))W_l(\phi(y))\ \text{dx dy} \\ &= -\int \left(\int\ \text{div}_x\left(\nabla\phi(y) e^{-\frac{\|x-y\|^2}{d^2}} W_l(\phi(x))W_l(\phi(y))\right)\ \text{dy}\ \right)\phi_t(x)\ \text{dx} \\ &\quad -\int \left(\int\ \text{div}_y\left(\nabla\phi(x) e^{-\frac{\|x-y\|^2}{d^2}} W_l(\phi(x))W_l(\phi(y))\right)\ \text{dx}\ \right)\phi_t(y)\ \text{dy} \\ &= -2\int \left(\int\ \text{div}_x\left(\nabla\phi(y) e^{-\frac{\|x-y\|^2}{d^2}} W_l(\phi(x))W_l(\phi(y))\right)\ \text{dy}\ \right)\phi_t(x)\ \text{dx} \\ &= 2\int \left(\int \left(\frac{2(x-y)}{d^2}\cdot\nabla\phi(y) e^{-\frac{\|x-y\|^2}{d^2}} W_l(\phi(x))W_l(\phi(y))\right)\ \text{dy}\ \right)\phi_t(x)\ \text{dx} \\ &\quad -2\int \left(\int \left(\nabla\phi(y)\cdot\nabla\phi(x) e^{-\frac{\|x-y\|^2}{d^2}} W_l'(\phi(x))W_l(\phi(y))\right)\ \text{dy}\ \right)\phi_t(x)\ \text{dx}.\end{aligned}$$

The second equality is simply integration by parts and the last equality is true by a change of variables. For the second subterm, a similar trick yields

$$\begin{aligned}\text{Term}_{2\text{b}} = &\iint \nabla\phi(x)\cdot\nabla\phi(y)\ e^{-\frac{\|x-y\|^2}{d^2}} \\ &\qquad [W_l'(\phi(x))W_l(\phi(y))\phi_t(x)+W_l(\phi(x))W_l'(\phi(y))\phi_t(y)]\ \text{dx dy} \\ = &\iint \nabla\phi(x)\cdot\nabla\phi(y)\ e^{-\frac{\|x-y\|^2}{d^2}} W_l'(\phi(x))W_l(\phi(y))\phi_t(x)\ \text{dx dy} \\ &+\iint \nabla\phi(x)\cdot\nabla\phi(y)\ e^{-\frac{\|x-y\|^2}{d^2}} W_l(\phi(x))W_l'(\phi(y))\phi_t(y)\ \text{dx dy} \\ = &2\int \left(\int \nabla\phi(x)\cdot\nabla\phi(y)\ e^{-\frac{\|x-y\|^2}{d^2}} W_l'(\phi(x))W_l(\phi(y))\ \text{dy}\ \right)\phi_t(x)\ \text{dx}.\end{aligned}$$

In this form we can combine both of the subterms together to get (with some cancellation)

$$\text{Term}_2 = -\frac{4\mu}{d^2}\int \left(\int \left((x-y)\cdot\nabla\phi(y) e^{-\frac{\|x-y\|^2}{d^2}} W_l(\phi(x))W_l(\phi(y))\right)\ \text{dy}\ \right)\phi_t(x)\ \text{dx}.$$

Each of the terms above separate the time derivative of ϕ from the main part of the integrand. Factoring out ϕ_t and combining all the computed terms yields

$$\begin{aligned}
&\partial_t \bar{E}(\phi(t,-)) \\
&= -\int \Big[\operatorname{div}\left(\frac{\nabla\phi}{|\nabla\phi|}\right) + \gamma\left((f-c_2)^2-(f-c_1)^2\right) \\
&\qquad + \frac{4\mu}{d^2} W_l(\phi) \int (x-y)\cdot\nabla\phi(y) e^{-\frac{\|x-y\|^2}{d^2}} W_l(\phi(y))\ \mathrm{dy}\ \Big]\phi_t(x)\ \mathrm{dx} \\
&= -\int \phi_t^2\ \mathrm{dx} \\
&\leq 0,
\end{aligned}$$

because ϕ satisfies equation (2.7) and $|\nabla\phi| = 1$ a.e. □

The argument above holds (with some additional work) for the original evolution equation (equation (2.6)) and the model (equation (2.3)). For clarity, we state it below.

THEOREM 2.3. *Let $\phi(t,x) \in C^1([0,T]; W^{1,\infty}(\Omega))$ be the solution to equation (2.6) with Neumann boundary conditions. Then, for all $t > 0$, we have $\partial_t E(\phi, c_1, c_2) \leq 0$.*

In the case of the original PDE, the energy is minimized by the evolution of ϕ and the variables c_1 and c_2.

2.3. Parameters. Altogether this model has several (positive) parameters, γ, μ, d, and l. Parameter d determines the region of nonlocality for the topology preserving term, specifically, the neighborhood defined in the topological term grows with d. Because the function ϕ remains close to a signed distance function, parameter l determines the characteristic distance (in terms of pixel size) between any two points on the curve. For our experiments, the parameters were set to $d = 4$ and $l = 1$. The energy balancing parameters γ and μ determine the curve structure. If μ is small relative to γ, then the resulting evolution will undergo topological changes. In practice, keeping μ close to 1 produces appropriate results. The parameter can be weakened in order to encourage a particular genus with some flexibility (allowing small amounts of deviation of topology from the initial curve). Without tuning of the parameters, the model will encourage the topology of the curve to remain close to the initial structure.

There is an additional parameter k which is used to accelerate the evolution and avoid local minima. This is not always necessary, but may be more practical in applications. In the general level set framework, it is common to add a balloon term $k|\nabla\phi|$, for constant k, which helps to shrink or grow the curve (depending on the sign of k). For our dynamics, the additional term would force equation (2.7) out of the true steady state, for non-zero k. In order to avoid this effect, the parameter can be made time-dependent $k(t)$, with the condition that $k(t) = 0$ for all $t > T$. This is done in some numerical experiments to accelerate the curve towards the edge set.

3. Numerical method

We set the time step to dt and the space step dx = 1 (in the equations below, we drop dx). To solve equation (2.7) to steady state, we use an additive operator splitting scheme as in [10]. The discretized equation is below:

$$\phi^{n+1} = \frac{1}{2}\sum_p (I - 2\mathrm{dt} A_p(\phi^n))^{-1} \Big(\phi^n + \mathrm{dt}\ \gamma\left((f-c_2)^2-(f-c_1)^2\right)$$

$$+4\frac{\mathrm{dt}\ \mu}{d^2}W_l(\phi^n)\int_\Omega (x-y)\cdot\nabla\phi^n(y)e^{-\frac{\|x-y\|^2}{d^2}}W_l(\phi^n(y))\ \mathrm{dy}\Big), \tag{3.1}$$

where p is the direction (x and y) and a vectorial representation of ϕ^n is used via concatenation of rows, for instance. The operator $A_p := (a_{ij})$ is defined pixel-wise as follows:

$$a_{ij}(\phi) = \begin{cases} |\nabla\phi|_i\left(\frac{2}{|\nabla\phi|_i+|\nabla\phi|_j}\right), & \text{if } j\in\mathcal{N}(i),\\ -|\nabla\phi|_i\sum_{k\in\mathcal{N}(i)}\left(\frac{2}{|\nabla\phi|_i+|\nabla\phi|_k}\right), & \text{if } j=i,\\ 0, & \text{otherwise,}\end{cases} \tag{3.2}$$

where $\mathcal{N}(i)$ is the neighborhood around i (adjacent pixels). For each p, the system can be solved via the Thomas algorithm, because it is a strictly diagonally dominant tridiagonal linear system. The resulting method has linear complexity at each time step. If one considers the method without the topological force, then it can be shown that the discretization is unconditionally stable.

The dimensional generalizations are direct, for example, the 3D discretized equation is below:

$$\begin{aligned}\phi^{n+1} = &\frac{1}{3}\sum_p (I-3\mathrm{dt}A_p(\phi^n))^{-1}\Big(\phi^n+\mathrm{dt}\ \gamma\big((f-c_2)^2-(f-c_1)^2\big)\\ &+4\frac{\mathrm{dt}\ \mu}{d^2}W_l(\phi^n)\int_\Omega (x-y)\cdot\nabla\phi^n(y)e^{-\frac{\|x-y\|^2}{d^2}}W_l(\phi^n(y))\ \mathrm{dy}\Big).\end{aligned} \tag{3.3}$$

One example of segmentation using our algorithm in 3 dimensions is provided.

Because the topological term must have the level set function close to a signed distance function, re-initialization is required. Following the method in [14], we iterate the following systems to convergence:

$$\psi^0 := \phi^n, \tag{3.4}$$

$$\psi_{ij}^{k+1} = \begin{cases}\psi_{ij}^k - \mathrm{dt}\left(\mathrm{sign}(\psi_{ij}^0)|\psi_{ij}^k|-D_{ij}\right), & \text{if } (i,j)\in\Lambda,\\ \psi_{ij}^k - \mathrm{dt}\ \mathrm{sign}(\psi_{ij}^0)G(\psi)_{ij}, & \text{otherwise,}\end{cases} \tag{3.5}$$

where the set Λ contains all (i,j) such that

$$\phi_{ij}^n\ \phi_{i+1,j}^n<0,\quad \phi_{ij}^n\ \phi_{i,j+1}^n<0,\quad \phi_{ij}^n\ \phi_{i-1,j}^n<0,\quad \text{or}\quad \phi_{ij}^n\ \phi_{i,j-1}^n<0.$$

In equation (3.5), D_{ij} is the numerical distance to $\mathcal{C}$ and can be calculated to be

$$D_{ij} = \frac{\psi_{ij}^0}{\sqrt{(D_x^0\psi_{ij}^0)^2+(D_y^0\psi_{ij}^0)^2}}, \tag{3.6}$$

where D^0 is the central difference operator. The upwind discretized re-initialization equation is given by

$$G(\psi)_{ij} := \begin{cases}\sqrt{\max\left((D_x^-\psi_{ij})_+^2,(D_x^+\psi_{ij})_-^2\right)+\max\left((D_y^-\psi_{ij})_+^2,(D_y^+\psi_{ij})_-^2\right)}-1, & \text{if } \psi_{ij}>0,\\ \sqrt{\max\left((D_x^-\psi_{ij})_-^2,(D_x^+\psi_{ij})_+^2\right)+\max\left((D_y^-\psi_{ij})_-^2,(D_y^+\psi_{ij})_+^2\right)}-1, & \text{if } \psi_{ij}<0,\end{cases}$$

where D^+ and D^- are the forward and backward differences, $f_+ := \max(f,0)$, and $f_- := \min(f,0)$. Once this iterative process converges we assign $\phi^n := \psi^\infty$ and continue

the evolution. The re-initialization is only done for a few iterations, for example, when n is a multiple of 50.

It should be noted that from [14], we know that this method's error is independent of the number of iterations, therefore the re-initialization process does not change the location of the curve. This is particularly important for the topology preservation, because the drifting caused by some re-initialization algorithms could change the results.

4. Results

The method is tested on several synthetic and real images containing various features. We provide a three dimensional result using the current algorithm as well as a possible extension for textured images. For the noisy images presented here, the noise variance is reported as the percent of the maximum intensity value of the given image.

4.1. Two dimensional examples. In figure 4.1 the algorithm is tested on a synthetic image containing two black discs on a white background. Noise is added in order to test the algorithms ability to preserve topology with highly corrupted images. As the curve evolves, it first captures part of the boundary of the discs then shrinks inward along the edges. The steady state solution resembles a bent dumbbell and is homeomorphic to the initial curve.

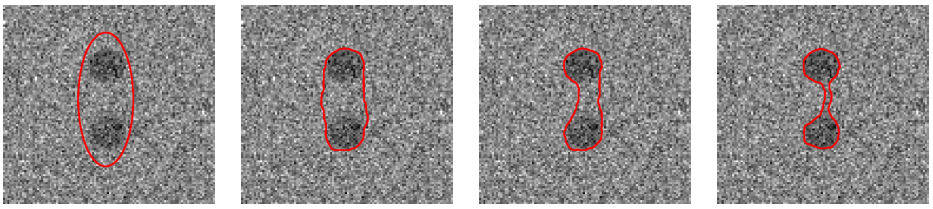

(a) Initial (b) Iteration= 200 (c) Iteration= 600 (d) Final (steady state), Iteration= 900

FIG. 4.1. *Our algorithm applied to the two discs example with* 70% *noise. The model parameters are set to* $\gamma = 0.195$ *and* $\mu = 0.4$.

For comparison to existing methods, we test our algorithm on the Hand image in figure 4.2. As the curve grows outward along each digit, each segment evolves separately. The steady state solution contains one continuous curve. Similar results can be found in [7] and in [10] for the noise-free case only. The addition of the large amount of noise further connects the digits, making the segmentation more complicated than in the noise-free case.

In figure 4.3, the algorithm is tested on a photograph of a bear. The image is highly textured, which can cause issues with gradient-based edge detectors. The curve locates the boundary of the bear without capturing the nose or grass (whose mean is closer to the background).

For the next few examples, the algorithm is tested on MRI scans of a human brain with Gaussian noise. In the first image (figure 4.4), the curve quickly locates the boundary of the brain (within 90 iterations), and continues to grow inward to refine the detection. In the other two images (figure 4.5 and 4.6), with the choice of initialization, the curve grows along the boundary of the object as well as shrinks

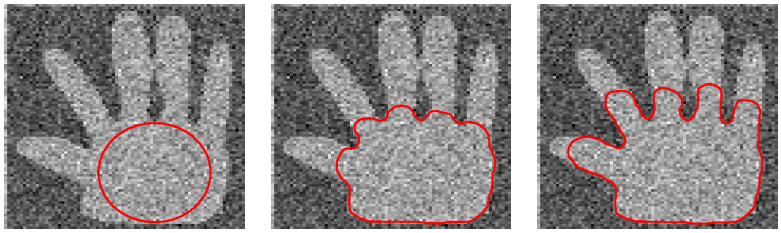

(a) Initial (b) Iteration= 100 (c) Iteration=200

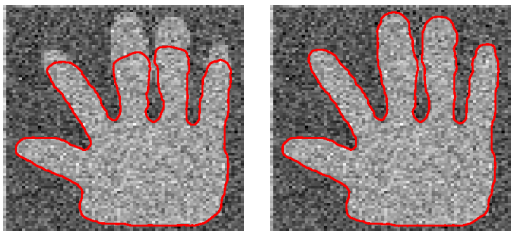

(d) Iteration=300 (e) Final (steady state), Iteration=400

FIG. 4.2. *Our algorithm applied to the Hand image with* 15% *noise. The model parameters are set to* $\gamma = 2.2$ *and* $\mu = 0.5$.

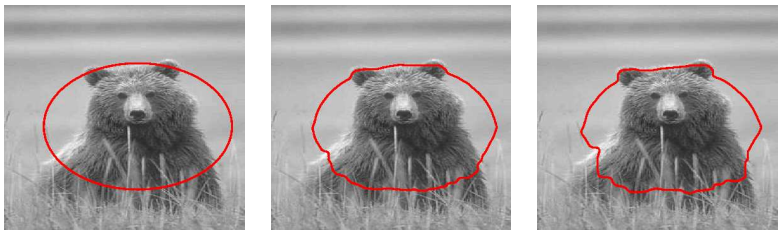

(a) Initial (b) Iteration= 100 (c) Iteration= 200

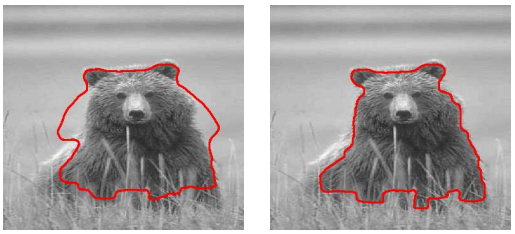

(d) Iteration= 400 (e) Final, iteration= 800

FIG. 4.3. *Our algorithm applied to the highly textured Bear photograph. The model parameters are set to* $\gamma = 3$ *and* $\mu = 0.8$.

within the small regions. The steady state solutions are all homeomorphic to the initial condition as well as contain the fine details of the detected object.

In figure 4.7, we apply the algorithm from [10] to two noisy images to compare the results. In both cases, the curve is initialized the same way as in our corresponding examples, and the parameters are optimized manually. In figure 4.7(a), the curve is stuck in a local minimum and does not locate many of the edges. In figure 4.7(b), the

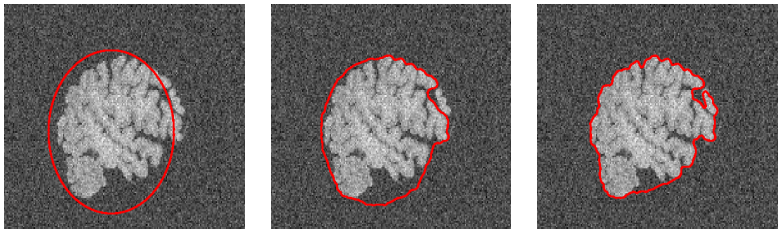

(a) Initial (b) Iteration=60 (c) Iteration=90

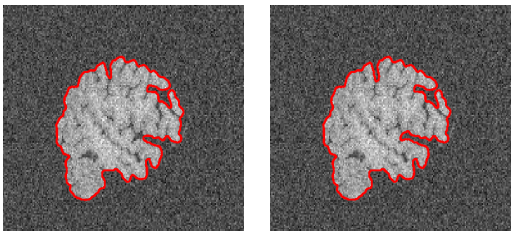

(d) Iteration=180 (e) Final, Iteration=270

FIG. 4.4. *Our algorithm applied to an MRI scan of a brain. The model parameters are set to* $\gamma = 1.45$ *and* $\mu = 0.5$.

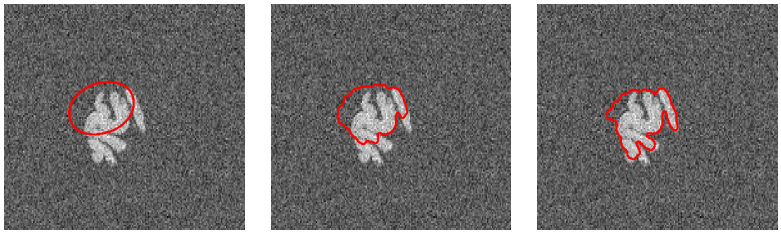

(a) Initial (b) Iteration= 20 (c) Iteration=40

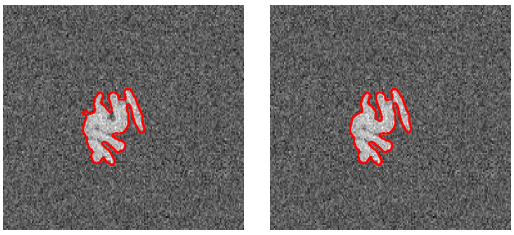

(d) Iteration=80 (e) Final, Iteration=110

FIG. 4.5. *Our algorithm applied to an MRI scan of a brain. The model parameters are set to* $\gamma = 2$ *and* $\mu = 1.2$.

curve finds the correct outer edge, but because of the high level of noise, is unable to locate the interior structures.

4.2. Three dimensional examples. As a proof of concept, we provide a 3D example using an MRI brain scan in figure 4.8. By monitoring the Euler characteristic of the zero level set function, we can numerically verify that the structure is preserved. From the two different perspectives of the steady state solution displayed in figure 4.8,

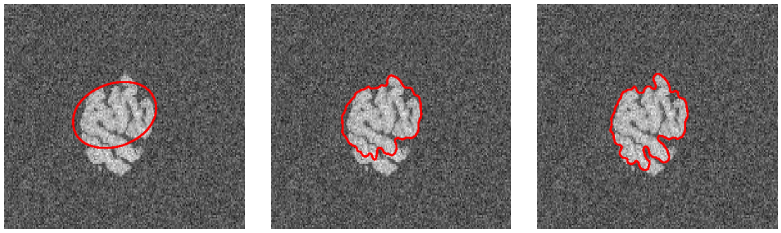

(a) Initial (b) Second, iteration= 10 (c) Third, iteration= 20

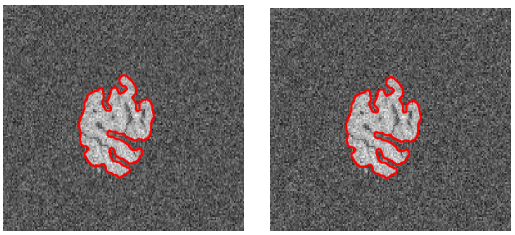

(d) Final, iteration= 60 (e) Final, iteration= 120

FIG. 4.6. *Our algorithm applied to an MRI scan of a brain. The model parameters are set to* $\gamma = 2$ *and* $\mu = 2$.

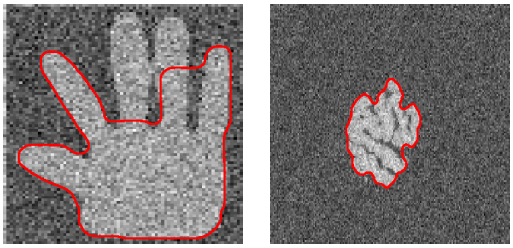

(a) Hand image (b) MRI scan of a brain

FIG. 4.7. *Results of the method in [10] applied to the hand and MRI scan of a brain. The resulting curve on the hand image is stuck in a local minimum. The curve in the brain image is able to locate the outer edges, but cannot locate the interior ones.*

the finer boundary structures can be seen as well as the crevasses. In the 3D case, to accelerate the convergence to steady state, we add the term $k(t)|\nabla\phi|$ to the evolution equation and set $k(t) = 0.05$ for $t < 400$ and $k(t) = 0$ otherwise.

4.3. Extensions. The regional terms used in equation (2.3) fit the data to the means in each region; however, it is possible to fit the data to any probabilistic model. For textured images, the authors of [13] proposed modeling the regional intensity values as samples from a Gaussian distribution. Using the regional term from [13], our model can be extended to the following:

$$\min_{\phi,c_1,c_2,\sigma_1,\sigma_2} E_G(\phi,c_1,c_2,\sigma_1,\sigma_2)$$
$$= \int_\Omega \delta(\phi)|\nabla\phi| \; + \mu \; T(\phi) + \gamma \int_\Omega \left(\log(\sigma_1) + \frac{(f-c_1)^2}{\sigma_1}\right) H(\phi)$$

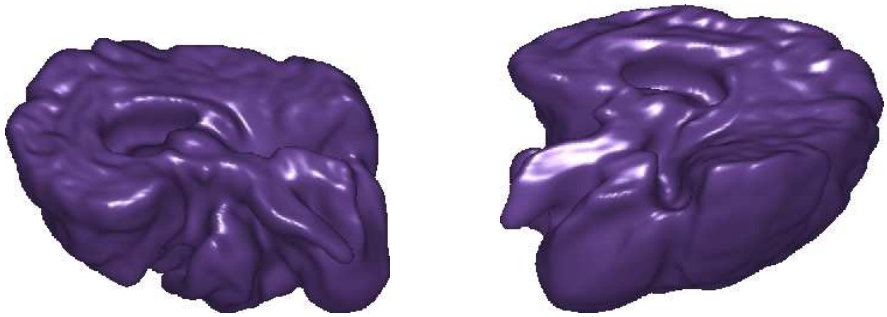

(a) First View (b) Second View

FIG. 4.8. *Our algorithm applied to a 3D MRI scan of a brain. The model parameters are set to* $\gamma = 1 \times 10^{-6}$ *and* $\mu = 0.2$.

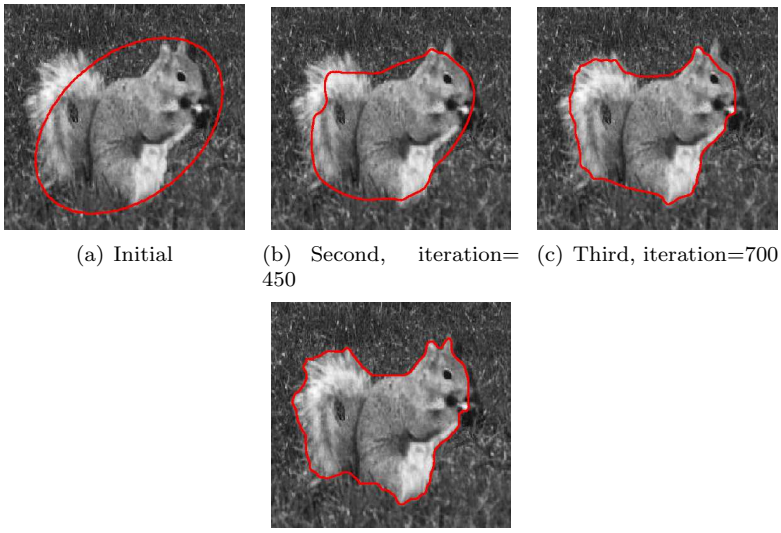

(a) Initial (b) Second, iteration= 450 (c) Third, iteration=700

(d) Final, iteration= 5000

FIG. 4.9. *Our algorithm applied to a 3D MRI scan of a brain. The model parameters are set to* $\gamma = 2.8 \times 10^{-5}$ *and* $\mu = 0.3$.

$$+\left(\log(\sigma_2)+\frac{(f-c_2)^2}{\sigma_2}\right)H(-\phi)\ \mathrm{dx}. \tag{4.1}$$

As a proof of concept, we test this extension on an image of a squirrel in figure 4.9. In order to avoid local minima, we include a balloon forcing term with coefficient equal to 0.12. Because the foreground and background texture are seemingly random, modeling their intensity values as Gaussian with different parameters seems to capture the correct boundary.

5. Conclusion

We have proposed a region based topology preserving active contours model. Unlike previous work on topology preserving segmentation, our method is not depen-

dent on an edge detector for pre-segmenting the image. Also, as demonstrated in the results, our method handles noisy and highly textured images well. For further applications, the model can easily be extended by either including a geodesic length term in place of the standard length or by changing the regional forces.

Acknowledgement. This research was supported by the UC Lab Fees Research Grant 12-LR-236660 and NSF DMS 1217239. H. Schaeffer was supported by the Department of Defense (DoD) through the National Defense Science and Engineering Graduate Fellowship (NDSEG). N. Duggan would like to acknowledge the support of the Irish Research Council (formerly the Irish Research Council for Science, Engineering and Technology) and the contribution of Dr. Martin Glavin and Dr. Edward Jones of Electrical and Electronic Engineering at the National University of Ireland, Galway in the completion of her research.

REFERENCES

[1] O. Alexandrov and F. Santosa, *A topology-preserving level set method for shape optimization*, J. Comput. Phys., 204(1), 121–130, 2005.
[2] R. Caselles, V. Kimmel, and G. Sapiro, *Geodesic active contours*, Inter. J. Comput. Vision, 22(1), 61–79, 1997.
[3] T.F. Chan, B.Y. Sandberg, and L.A. Vese, *Active contours without edges for Vector-Valued images*, J. Visual Commun. Image Represent., 11(2), 130–141, 2000.
[4] T.F. Chan and L.A. Vese, *Active contours without edges*, IEEE Trans. Image Proc., 10(2), 266–277, 2001.
[5] G. Chung and L.A. Vese, *Image segmentation using a multilayer level-set approach*, Comput. Vis. Sci., 12(6), 267–285, 2008.
[6] L.C. Evans and R.F. Gariepy, *Measure Theory and Fine Properties of Functions*, CRC Press, 1992.
[7] X. Han, C. Xu, and J.L. Prince, *A topology preserving level set method for geometric deformable models*, IEEE Trans. Pattern Anal. Machine Int., 25(6), 755–768, 2003.
[8] M. Kass, A. Witkin, and D. Terzopoulos, *Snakes: Active contour models*, Inter. J. Comput. Vision, 1(4), 321–331, 1988.
[9] S. Kichenassamy, A. Kumar, P. Olver, A. Tannenbaum, and A. Yezzi, *Gradient flows and geometric active contour models*, in Proceedings of the Fifth International Conference on Computer Vision, 810–815, 1995.
[10] C. Le Guyader and L.A. Vese, *Self-repelling snakes for topology-preserving segmentation models*, IEEE Trans. Image Proc., 17(5), 767–779, 2008.
[11] D. Mumford and J. Shah, *Optimal approximations by piecewise smooth functions and associated variational problems*, Commun. Pure Appl. Math., 42(5), 577–685, 1989.
[12] S. Osher and J.A. Sethian, *Fronts propagating with curvature-dependent speed: Algorithms based on Hamilton-Jacobi formulations*, J. Comput. Phys., 79(1), 12–49, 1988.
[13] M. Rousson and R. Deriche, *Adaptive segmentation of vector valued images*, in Geometric Level Set Methods in Imaging, Vision, and Graphics, 195–205, 2003.
[14] G. Russo and P. Smereka, *A remark on computing distance functions*, J. Comput. Phys., 163(1), 51–67, 2000.
[15] H. Schaeffer, *Active arcs and contours*, UCLA CAM Report, 12–54, 2012.
[16] H. Schaeffer and L. Vese, *Active contours with free endpoints*, J. Math. Imaging and Vision, 49(1), 20–36, 2014.
[17] L.A. Vese and T.F. Chan, *A multiphase level set framework for image segmentation using the Mumford and Shah model*, Inter. J. Comput. Vision, 50(3), 271–293, 2002.